batteries

MDPI

Article

Diphenylphosphoryl Azide as a Multifunctional Flame Retardant Electrolyte Additive for Lithium-Ion Batteries

Zhirui Li [1], Longfei Han [1], Yongchun Kan [1,*], Can Liao [2,*] and Yuan Hu [1]

[1] State Key Laboratory of Fire Science, University of Science and Technology of China, Hefei 230026, China; lizhirui@mail.ustc.edu.cn (Z.L.); hlongfei@mail.ustc.edu.cn (L.H.); yuanhu@ustc.edu.cn (Y.H.)
[2] College of Materials Science and Engineering, Fuzhou University, Fuzhou 350108, China
* Correspondence: yckan@ustc.edu.cn (Y.K.); liaocan@fzu.edu.cn (C.L.)

Abstract: Graphite anode materials and carbonate electrolyte have been the top choices for commercial lithium-ion batteries (LIBS) for a long time. However, the uneven deposition and stripping of lithium cause irreversible damage to the graphite structure, and the low flash point and high flammability of the carbonate electrolyte pose a significant fire safety risk. Here, we proposed a multifunctional electrolyte additive diphenylphosphoryl azide (DPPA), which can construct a solid electrolyte interphase (SEI) with high ionic conductivity lithium nitride (Li_3N) to ensure efficient transport of Li^+. This not only protects the artificial graphite (AG) electrode but also inhibits lithium dendrites to achieve excellent electrochemical performance. Meanwhile, the LIBS with DPPA offers satisfactory flame retardancy performance. The AG//Li half cells with DPPA-0.5M can still maintain a specific capacity of about 350 mAh/g after 200 cycles at 0.2 C. Its cycle performance and rate performance were better than commercial electrolyte (EC/DMC). After cycling, the microstructure surface of the AG electrode was complete and flat, and the surface of the lithium metal electrode had fewer lithium dendrites. Importantly, we found that the pouch cell with DPPA-0.5M had low peak heat release rate. When exposed to external conditions of continuous heating, DPPA significantly improved the fire safety of the LIBS. The research of DPPA in lithium electrolyte is a step towards the development of safe and efficient lithium batteries.

Keywords: diphenylphosphoryl azide; solid electrolyte interphase; lithium nitride; flame retardant; electrolyte additive

Citation: Li, Z.; Han, L.; Kan, Y.; Liao, C.; Hu, Y. Diphenylphosphoryl Azide as a Multifunctional Flame Retardant Electrolyte Additive for Lithium-Ion Batteries. *Batteries* **2024**, *10*, 117. https://doi.org/10.3390/batteries10040117

Academic Editor: Atsushi Nagai

Received: 25 February 2024
Revised: 23 March 2024
Accepted: 27 March 2024
Published: 30 March 2024

1. Introduction

With the advancement of technology and the changing world energy pattern, the development of advanced energy storage equipment is thriving [1,2]. Among them, lithium batteries have become an indispensable energy device due to their advantages of convenience, cleanliness and high efficiency. They are widely used in mobile phones, computers, electric vehicles and other fields [3–5]. In the face of environmental pollution and energy crisis, China has proposed the goal of "carbon peaking and carbon neutrality", which will lead to the rapid development of lithium batteries. Although there are many types of lithium batteries, lithium-ion batteries (LIBS) have still been the most important commercial lithium batteries for a long time. Layered graphite (theoretical specific capacity 372 mAh/g) is widely used as a commercial anode for LIBS with its advantages of lightweight, high conductivity and low potential. The charge and discharge process are realized through the insertion and removal of Li^+ in the layers [6,7]. However, the compatibility between graphite anode and electrolyte is poor due to the uneven SEI. The SEI is destroyed, resulting in continuous electrolyte consumption, graphite laminate volume expansion and irreversible damage [8–13]. This leads to the loss of electrochemical stability and deterioration of electrochemical performance of the battery, particularly at high current density. Low ionic conductivity in rapid charging can easily lead to graphite anode lithium evolution.

The accumulated "dead lithium" and the electrolyte carry out a parasitic side reaction, resulting in irreversible SEI destruction [14–17]. Electrolyte is the blood of LIBS; the carbonate electrolyte is commonly used in commercial LIBS [18]. However, the low flash point and high flammability of commercial electrolytes are major factors contributing to lithium battery safety accidents [19,20]. As people's demand for the energy density of lithium batteries increases, battery safety accidents have occurred frequently in recent years. Extrusion, acupuncture, high temperature as well as the lithium dendrites and other problems will cause the battery to short-circuit, leading to thermal runaway and explosion accidents, which pose great threats to people's lives and property safety [20–22].

Many scientists have been working on improving the stability of graphite electrode by constructing SEI, graphite functionalization, electrode structure design and so on [6,7]. The SEI is formed by the reaction of electrode with electrolyte at the solid–liquid phase interface during the first charge and discharge process of lithium batteries. The SEI is mainly composed of various inorganic components, such as lithium carbonate (Li_2CO_3), lithium fluoride (LiF), lithium oxide (Li_2O) and lithium hydroxide (LiOH), and some organic components, such as alkyl lithium carbonate ($ROCO_2Li$), allow Li^+ to move freely, while electrons cannot [23–25]. In recent years, lithium nitride (Li_3N) has emerged as a promising component of artificial protective layers due to its low conductivity ($<10^{-12}$ S/cm), high ionic conductivity (up to 10^{-3} S/cm) and high Young's modulus (up to 48 GPa) [26,27]. Cui et al. constructed a pinhole-free and ion-conductive α-Li_3N film by directly reacting molten lithium foil with nitrogen [28], Chen et al. designed a multifunctional protective layer using N_2 plasma activation to obtain a flower-like Li_3N layer on the surface of Li metal [29], and Goodenough et al. modified the surface of lithium with Li_3N [30]. Their studies have proved that a Li_3N layer can regulate the uniform deposition and efficient transport of Li^+. Similarly, the construction of Li_3N-rich SEI on the electrode surface will also play a key role in the uniform deposition and stripping of lithium [31–37]. In this study, diphenylphosphoryl azide (DPPA) was proposed as a multifunctional additive for LIBS. The density functional theory (DFT) showed that DPPA preferentially reacts at the solid–liquid interface to construct a SEI compared to commercial electrolyte components [20,36,38–40]. DPPA can construct a stable Li_3N-rich SEI with high ionic conductivity, which can regulate the uniform deposition/stripping of Li^+ and improve the transportation efficiency of Li^+. The Li_3N- rich SEI enables Li^+ to move more freely in the graphite interlayer structure and reduce the graphite interlayer expansion and fracture, making the electrochemical performance more stable. AG//Li half cells with DPPA-0.5M can still maintain a specific capacity of about 350 mAh/g after 200 cycles at 0.2 C, and the effect of Li_3N-rich SEI is more obvious in the rate performance test. Meanwhile, the uniform current density distribution on the surface of Li_3N-rich SEI inhibits the generation of lithium dendrites. To further verify the effect of Li_3N-rich SEI, X-ray photoelectron spectroscopy (XPS) surface element analysis and scanning electron microscopy (SEM) observation were performed. After the cycle and rate performance tests of LFP//Li half cells, it was found that the appropriate amount of DPPA did not have a negative effect on the LFP//Li system.

Liquid electrolyte and separator are the firewood of battery combustion [20,22,41]. Adding flame retardant additives to block battery combustion is a simple and efficient way to improve safety. In this work, we tested the flame retardancy performance and self-extinguishing time (SET) of the electrolyte with different concentrations of DPPA. DPPA can inhibit the flame effectively. It is mainly because the PO· and PO_2· free radicals generated by DPPA can capture H· and OH· free radicals during the combustion process to block the free radical chain reaction to stop the combustion. The study showed that compared with commercial electrolyte, the pouch cell with DPPA had low peak heat release rate. This proves that DPPA improved the fire safety of the LIBS.

Therefore, the advantages of DPPA are as follows: (1) DPPA can participate in the construction of a stable and high ionic conductivity Li_3N-rich SEI, protect the electrode, and improve the electrochemical performance; (2) DPPA can block the free radical chain reaction to prevent the flame and improve the fire safety of the LIBS; (3) the economic cost is low, and

it is easy to achieve large-scale commercialization. DPPA is a multifunctional electrolyte additive that can simultaneously meet the high safety and excellent electrochemical stability of LIBS. It provides a simple and efficient method for the future development of safe and efficient LIBS.

2. Experimental Section

2.1. Raw Materials

Lithium hexafluorophosphate ($LiPF_6$, battery grade) was purchased from Dongguan shanshan Co., Ltd. (Dongguan, China). Diphenylphosphoryl azide (DPPA, 97%, AR) was provided kindly by Shanghai Aladdin Bio-Chem Technology Co., Ltd. (Shanghai, China). The commercial separator (Celgard 2325) came from the Celgard company of America (Charlotte, NC, USA). The commercial electrolyte ethylene carbonate/dimethyl carbonate (EC/DMC) (1:1, *v*/*v*) containing 1 M $LiPF_6$ was supplied by Dodo chem (Suzhou, China). Lithium metal plates with the thickness of 0.5 mm (>99.5%, purity) were received from China Energy Lithium Co., Ltd. (Tianjin, China). The cathode materials of $LiFePO_4$ (LFP), anode materials of artificial graphite (AG), binder of Polyvinylidene fluoride (PVDF) and conductive additive of super P were purchased from Guangdong New Energy Technology Co., Ltd. (Guangzhou, China).

2.2. Electrolyte Preparation

To keep the concentration of $LiPF_6$ in the electrolyte at 1M after the addition of DPPA, we first prepared DPPA solution containing 1M $LiPF_6$ (DPPA was treated with 4Å molecular sieve for 48 h to remove trace water inside before use), and then mixed DPPA solution with EC/DMC evenly according to different mole ratios. Thus, the electrolytes with DPPA concentration of 0.1 M, 0.2 M, 0.5 M, 1.0 M and 1.5 M can be accurately prepared. These electrolytes were named DPPA-0.1M, DPPA-0.2M, DPPA-0.5M, DPPA-1.0M and DPPA-1.5M, respectively. These abbreviations will be used directly below.

2.3. Flame Retardant Tests of Electrolyte

The flame retardancy effect of different electrolytes was directly tested by ignition experiment. Meanwhile, to quantitatively study the flame retardancy performance of DPPA more accurately, we measured the self-extinguishing time (SET) of the electrolyte, which was obtained by normalizing the flame combustion time against the electrolyte mass. Thermogravimetric analysis (TGA, Q5000) was employed to detect the thermal stability of the electrolyte by the heating rate of 10 °C min^{-1} at nitrogen atmosphere. We used an electric heating board to continuously heat the pouch cells externally, recorded the entire heating process using a digital camera, recorded their temperature changes using a thermal imager and thermocouple, and tested their heat release and gas release using a cone calorimeter.

2.4. Electrochemical Measurements

Electrochemical impedance spectroscopy (EIS) was confirmed with a frequency range of 0.1–10^6 Hz at room temperature of 25 °C. Linear sweep voltammetry (LSV) was acquired with a scan rate of 1.0 mV s^{-1} between 2.0 V and 6.0 V. At a scan rate of 0.2 mV s^{-1}, cyclic voltammetry (CV) was carried out at the voltage range of 0–2.0 V. The above tests were conducted at Chenhua Autolab. At room temperature, the LFP//Li half cells and AG//Li half cells were charged and discharged at 0.2 C to determine the cycle performance. To assess the rate performance of the LFP//Li half cells and AG//Li half cells at room temperature, cells were charged and discharged at successive rates of 0.1 C, 0.2 C, 0.5 C, 1.0 C, 2.0 C, 4.0 C and 0.1 C. The above tests used the Land button battery test system.

2.5. Characterization

In order to clearly observe the lithium metal deposition and the morphology of artificial graphite anode after electrochemical cycle, scanning electron microscope (SEM) was

utilized. The surface elements of lithium metal and artificial graphite anode were analyzed by X-ray photoelectron spectroscopy (XPS) with an excitation source of monochromatized Al Ka (hv = 1486.6 eV) and a pass energy of 40 eV, and the test power was controlled at 150 W. All observed materials were disassembled in a glove box filled with argon and cleaned by DMC.

3. Results and Discussion

We first tested the flame retardancy effect of electrolytes with DPPA by ignition experiment. The experiment used non-combustible glass fiber discs to adsorb the same amount (200 μL) of EC/DMC, DPPA-0.5M and DPPA-1.0M, respectively. The whole experiment process was recorded by video shooting (the detailed process was recorded in Videos S1–S3, Supplementary Materials). As shown in Figure 1a, the EC/DMC commonly used in LIBS burn violently after ignition, the flame extinguished after the electrolyte burned out and the entire combustion process lasted 26 s, which showed poor safety. DPPA-0.5M could be ignited, but the flame was small, and the combustion process stopped abruptly in the 6th s; white smoke rose after the flame extinguished, which was because the flame retardant additive DPPA played a role in stopping the combustion. After the DPPA-1.0M was ignited, the fire was smaller than the DPPA-0.5M, and the flame naturally extinguished in the 2nd s. Figure 1b,c shows the TGA curves of the electrolytes in nitrogen and air, respectively; the mass loss of EC/DMC mainly comes from the volatilization of carbonate electrolyte and the thermal decomposition of lithium salt ($LiPF_6$). In air, $LiPF_6$ decomposes at 70 °C due to the presence of H_2O. In nitrogen, the H_2O is trace and $LiPF_6$ will not decompose until the temperature rises to 160 °C [42]. The thermal decomposition temperature of LiPF6 is marked in the curves. Compared with EC/DMC, DPPA has better thermal stability, and thermal weight loss occurs later in the heating process. It allows DPPA to better play a flame-retardant role without large amounts of volatilization. The thermal weight loss of DPPA-0.5M and ECDMC are similar. Above 50 °C, the electrolyte begins to volatilize, but thermal weight loss is faster in air because of O_2 and H_2O. To quantitatively investigate the flame retardancy of DPPA, we tested the SET values of EC/DMC and electrolytes containing different concentrations of DPPA, which were obtained by normalizing the flame burning time with the mass of the electrolyte. As shown in Figure 1d, the SET value of EC/DMC is about 165 s/g, and it decreases rapidly after adding DPPA. The SET decreases to about 20 s/g when the additive content is 0.5 M. As the content increases to 1.0 M, the SET is even closer to 0 s/g. The above experimental phenomena show that DPPA has a satisfactory flame retardancy effect. As shown in Figure 1e, the main mechanism of DPPA flame retardant is the free radical scavenging mechanism. In the combustion process, DPPA can produce a large number of free radicals containing phosphorous, such as PO· and PO_2·, and they can actively capture H· and HO· free radicals to weaken and cut off the combustion chain reaction, so as to achieve flame retardancy.

The effect of DPPA additive on the electrochemical performance of the battery system is one of our key research objects. As a satisfactory additive, DPPA can participate in the construction of SEI film, an important part of the electrochemical process of the battery system. As we all know, the SEI is an interface layer formed by the reaction between electrode and electrolyte at the solid–liquid interface during the first charge and discharge process of the LIBS. Li^+ is allowed to be freely embedded and removed, but other solvent molecules are not allowed to pass through [23–25]. It can exist stably in the organic electrolyte and have a crucial effect. The azide group of DPPA can play an important role in the construction of SEI. We found that DPPA can form a stable Li_3N-rich SEI with high ionic conductivity, and it can achieve the homogenization of current density on the electrode surface. It not only improves the ionic conductivity to achieve stable and efficient interfacial dynamics but also achieves smooth deposition of Li^+ to protect graphite anode and inhibit lithium dendrites [26,28,29,37]. To further verify our view, the lowest unoccupied molecular orbital (LUMO) level electron density diagrams of EC, DMC and DPPA were calculated

based on density functional theory (DFT) (Figure 2). It shows that DPPA has the lowest LUMO in the electrolyte, indicating that DPPA has a stronger tendency to have a reduction reaction compared with other components in the electrolyte. This will give DPPA priority in building SEI. It can be seen from the figure that the electron density of DPPA is mainly concentrated around one phosphorus atom and three nitrogen atoms. It indicates that phosphorus and nitrogen determine the electrochemical REDOX behavior of DPPA, and this result is consistent with the view of forming a Li_3N-rich SEI.

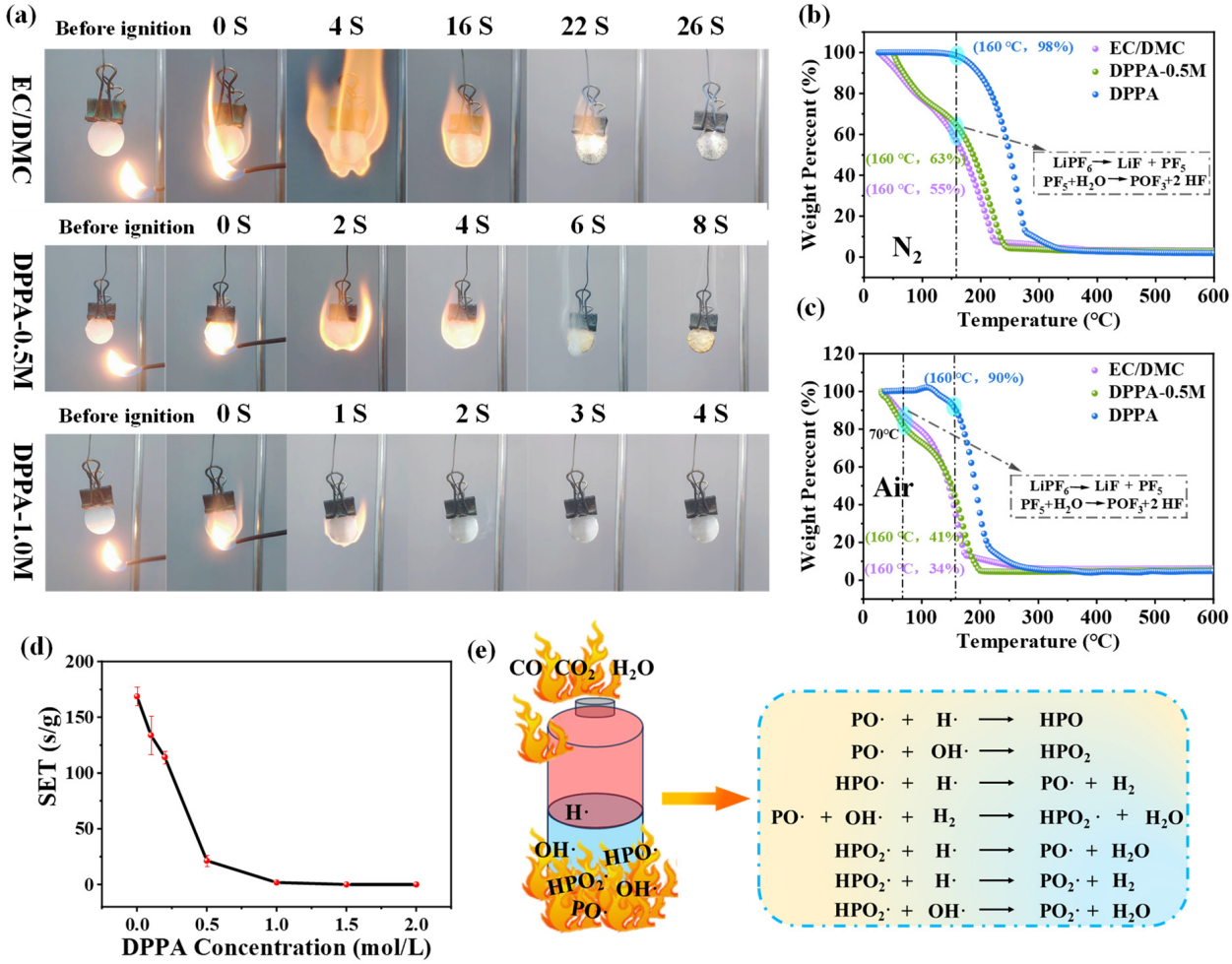

Figure 1. (**a**) The flame retardant test. TGA curves: (**b**) N_2, (**c**) Air. (**d**) SET test. (**e**) Schematic diagram of flame-retardant mechanism.

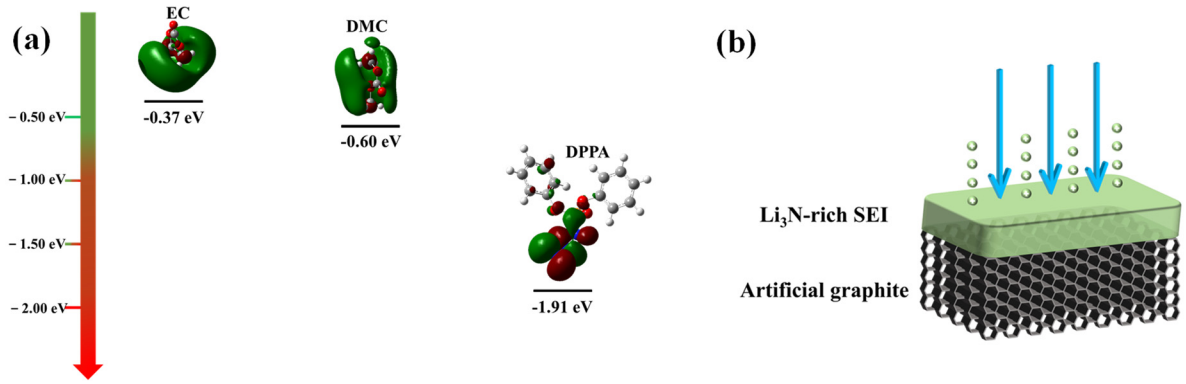

Figure 2. (**a**) LUMO energy calculation diagram of electrolyte composition and DPPA additive. (**b**) Diagram of Li_3N-rich SEI on the surface of graphite electrode.

Figure 3a shows the cycle performance of AG//Li half cells with different electrolytes, all of the cells have coulomb efficiency above 99%. Cells with EC/DMC can maintain a satisfactory charge specific capacity of 330 mAh/g at a current density of 0.2 C but show a slight downward trend after 200 cycles. This is a normal attenuation in the use of commercial batteries, due to the uneven diffusion of Li^+ in the graphite layer and the poor deposition and stripping of lithium. In contrast, cells with both DPPA-0.1M and DPPA-0.2M maintain a high specific charge capacity and do not show a negative decline after 200 cycles. When the DPPA concentration reaches 0.5 M, the specific charging capacity of the cells can reach about 350 mAh/g stably, which is far more than the commercial electrolyte. DPPA can build a Li_3N-rich SEI; Li_3N has high ionic conductivity (up to 10^{-3} S/cm) and high Young's modulus (up to 48 GPa), so a Li_3N-rich SEI is more stable and more conducive to Li^+ transport. Therefore, during the electrochemical cycle, cells with DPPA-0.5M can achieve efficient transport of Li^+, thereby improving coulomb efficiency and slowing down the attenuation of capacity. It can be observed from the capacity voltage curves (Figure 3b,c) that the cells with DPPA-0.5M have almost no capacity attenuation after 200 cycles, while the cells with EC/DMC have obvious capacity attenuation (capacity retention rate = 96.8%) under the same circumstances. However, the cycle performance of the cells with DPPA-1.0M is poor, and the specific charging capacity of the cells with DPPA-1.5M is only about 100 mAh/g. The SEI plays a key role in the battery electrochemical performance. According to the results of DFT calculation, DPPA is more inclined to build SEI on the electrode surface. We speculate that the deterioration of electrochemical performance of DPPA-1.5M is due to the formation of a too thick SEI. During the long cycle of the battery, a too thick SEI will continue to affect the desolvation process of lithium ions, resulting in poor electrochemical performance. We tested the rate performance of AG//Li half cells between 0.1 C and 4 C to meet the needs of practical applications. As shown in Figure 3d, the difference in rate performance between cells with different electrolytes is almost same as the difference in their cycle performance. Cells with DPPA-0.5M show very good rate performance compared with others, which shows that they can meet the needs of fast charging and fast discharging batteries. However, when the DPPA concentration reaches 1.5 M, it has a negative effect on the electrochemistry of the cells. The above experimental results show that adding appropriate DPPA additive to AG//Li systems can significantly and satisfactorily improve the capacity retention rate and rate performance. To test the effect of DPPA on the LFP//Li systems, we tested the cycle performance and rate performance of LFP//Li half cells with different electrolytes, as shown in Figure 3e,f. Their performance differences are not as obvious as the above AG//Li systems. In addition to the poor performance of DPPA-1.5M, as always, other cells with DPPA can maintain stable and close to or better than the electrochemical performance of cells with EC/DMC. It shows that DPPA can be compatible with LFP//Li systems, and the appropriate amount of addition will not cause negative effects.

The electrochemical performance is improved, which is attributed to the high ionic conductivity and stability of the Li_3N-rich SEI built by DPPA. It can homogenize the lithium flux on the electrode surface and promote the efficient transport and uniform diffusion of Li^+. We carried out impedance tests to observe the difference of ionic conductivity more directly. Figure 3g is the impedance spectrum of Steel sheet//Steel sheet cells with different electrolytes; Figure 3h shows the interface impedance curves of the AG//Li cells, and it clearly shows that the impedance gradually decreases with the increase of DPPA concentration in the electrolyte. The above test results are the most direct proof of the excellent electrochemical performance of DPPA. The electrolytes with DPPA have excellent wetting ability for a commercial separator, which makes it fast to infiltrate and fill in the battery system. Figure 3i shows the contact angle test results of EC/DMC and DPPA-0.5M. Two electrolytes were dropped to the commercial polyolefin separator (Celgard 2325), respectively. The contact angle of EC/DMC was 75°, and the contact angle of DPPA-0.5M was 62°. The complete contact angle test results are shown in Figure S1. Figure S2 also shows the wettability of different electrolytes on commercial separators. Equal amounts of

EC/DMC or DPPA-0.5M were dropped on two separators, respectively. After stopping for 2 s, clean and dry dust-free paper was used to wipe off the droplets. The DPPA-0.5M has stronger affinity and better wettability for the separator, so that it is easier to be compatible with the battery system. It is also good for improving Li^+ transport dynamics, a key driver of high ionic conductivity.

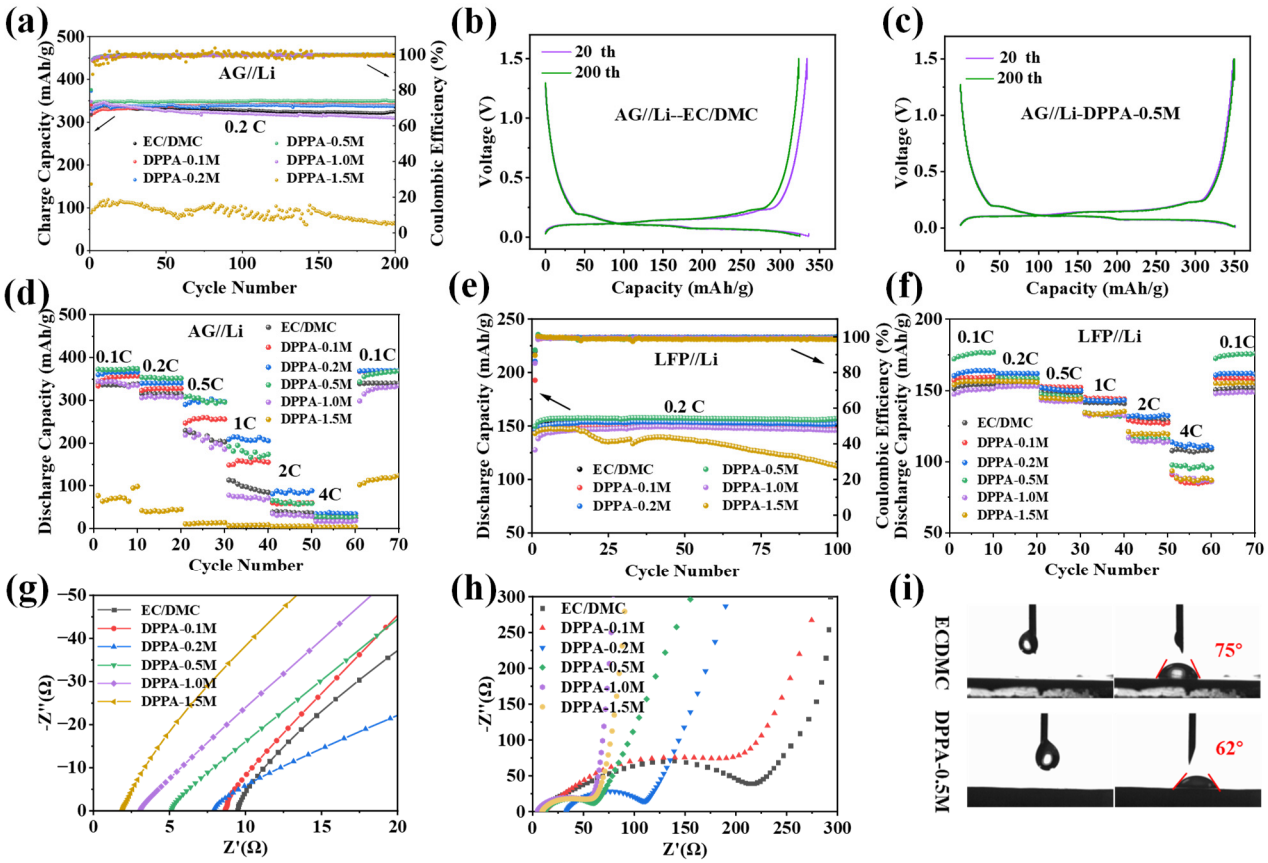

Figure 3. Cycle performance diagram of half cells with EC/DMC and electrolytes containing various concentrations of DPPA at 0.2C current density (**a**) AG//Li half cells and (**e**) LFP//Li half cells. Rate performance diagram of EC/DMC and electrolytes containing various concentrations of DPPA at current densities from 0.1C to 4C (**d**) AG//Li half cells and (**f**) LFP//Li half cells. Capacity voltage curves for the 20th and 200th cycles of the AG//Li half cells (**b**) EC/DMC (**c**) DPPA-0.5M. (**g**) Impedance spectrum of Steel sheet// Steel sheet cells with DPPA at different concentrations. (**h**) Nyquist diagram of AG//Li half cells with various concentrations of DPPA. (**i**) Digital photos of contact angle test of electrolytes.

To further understand the behavior of DPPA in the electrochemical process of the cells, LSV and CV were performed on the EC/DMC and electrolytes with DPPA. The electrochemical window curves of the electrolytes with and without DPPA are shown in Figure S3. The CV curves of AG//Li half cells with and without DPPA are shown in Figure S4. They show that during the first scanning cycle, the reduction peaks near 0.75 V and 2.0 V become more and more obvious and sharp with the increase of DPPA concentration, indicating that the reduction reaction of DPPA occurs at this time. This is consistent with the previously mentioned DPPA involvement in the formation of SEI. The subsequent second and third cycle recombination degree increases, and the REDOX peaks are sharper, which shows that the additive can be well adapted to the graphite electrode and improve the cyclic dynamics of the battery. However, things will develop in the opposite direction when they become extreme. As can be seen from Figure S3, the REDOX peaks become lower and wider. We estimate that the excessive DPPA leads to the formation of excessive SEI thickness, and the excessive DPPA molecules in the electrolyte

have a certain blocking effect on ion transfer. The above results are consistent with the electrochemical cycle.

In addition to satisfactory flame retardancy performance and excellent electrochemical performance, DPPA also has a certain protective effect on the electrode. Li^+ is deposited and stripped in the layered structure of the graphite anode through an intercalation mechanism. The uneven deposition and inefficient ion diffusion will cause damage to the graphite structure, and even lead to the collapse of the graphite layered structure. Meanwhile, under the influence of adverse factors such as the imbalance of lithium flux and the negative reaction inside the battery, the ordinary SEI is not stable enough. After the SEI is damaged, the electrolyte will contact the electrode again and continue to consume; the above results will damage the electrochemical performance (Figure 4a). The Li_3N-rich SEI constructed by DPPA is more stable. It can homogenize the lithium flux on the electrode surface, promote the efficient transport and uniform deposition of Li^+. It is conducive to the efficient insertion and removal of Li^+ in the graphite layer. Therefore, a Li_3N-rich SEI can slow down the damage of the graphite structure and play a certain protective role on the electrode. In the same way, efficient Li^+ transport can also inhibit the growth of lithium dendrites to improve the safety of batteries. Figure 4b is a comparison of the time–voltage curves of Li//Li batteries with EC/DMC and DPPA-0.5M, respectively. The Li//Li batteries with EC/DMC always have a higher potential, and their polarization voltage increases significantly when the battery cycle reaches about 280 h, which corresponds to the growth of lithium dendrites. In contrast, Li//Li batteries with DPPA-0.5M do not show obvious voltage polarization with the help of a Li_3N-rich SEI and can complete the work stably. The experimental results of Li//Li batteries' cycle show that a Li_3N-rich SEI can promote the uniform deposition of lithium and inhibit the growth of lithium dendrites effectively.

To observe the actual effect of DPPA additive on protecting the graphite anode and inhibiting lithium dendrites, SEM was used to observe the electrode microstructure of Li//Li batteries and AG//Li half cells after cycles with different electrolytes. As shown in Figure 5a,b, the Li anode of the Li//Li batteries with EC/DMC or DPPA-0.5M are compared. The surface of the former is full of messy and sharp lithium dendrites, while the surface of the latter has fewer lithium dendrites, showing regular blocky microscopic morphology. It directly reflects the obvious inhibition effect of a Li_3N-rich SEI on the growth of lithium dendrites. Figure 5c,d show the AG electrodes after 200 cycles in EC/DMC or DPPA-0.5M. The former has a rugged surface and damaged structure, the latter has a flat surface and complete structure. It is direct proof of the DPPA protection on the graphite structure. The differences of microscopic morphology on the electrode's surface are closely related to the Li_3N-rich SEI. On the lithium metal side, Li^+ achieves fast and efficient transfer and uniform deposit with the help of the Li_3N-rich SEI. It inhibits the tip effect to a certain extent, reduces the generation of dead lithium and inhibits the growth of lithium dendrites. On the graphite anode side, the stable Li_3N-rich SEI can guide the Li^+ to move more freely between the graphite layers to avoid excessive expansion and pulverization of the graphite structure. Efficient and uniform deposition and stripping of lithium can achieve the maximum protection of the graphite structure. DPPA protection of the graphite anode and inhibition of lithium dendrites are important reasons for the excellent cycle performance and rate performance of AG//Li half cells with DPPA-0.5M. To further investigate the composition of the SEI, XPS was used to characterize the electrode surface. Figure 5e,h show the P 2p spectra of Li electrodes and AG electrodes after 200 cycles with different electrolytes. $Li_xPO_yF_z$ has a peak of 136.8 eV and P-O has a peak of 133.9 eV; they are derived from $LiPF_6$ and DPPA. P-O bond can change the morphology and composition of the SEI; it is conducive to the formation of a thin and dense SEI layer [43]. Figure 5i,l show the N 1s spectra of different electrodes. Due to the addition of DPPA, Li_3N peak and LiN_xO_y peak are generated at 398.8 eV and 400.3 eV, respectively. They are generated by the reduction reaction of the azide group of DPPA during the construction of the Li_3N-rich SEI [20]. LiN_xO_y and Li_3N are lithium nitrogen compounds, and LiN_xO_y also has high ionic conductivity and is a favorable component in SEI, therefore we uniformly named

them as Li_3N-rich SEI [44,45]. The above experimental results prove the existence and significant role of a Li_3N-rich SEI (the content comparison of various elements in a SEI is shown in Figure S5).

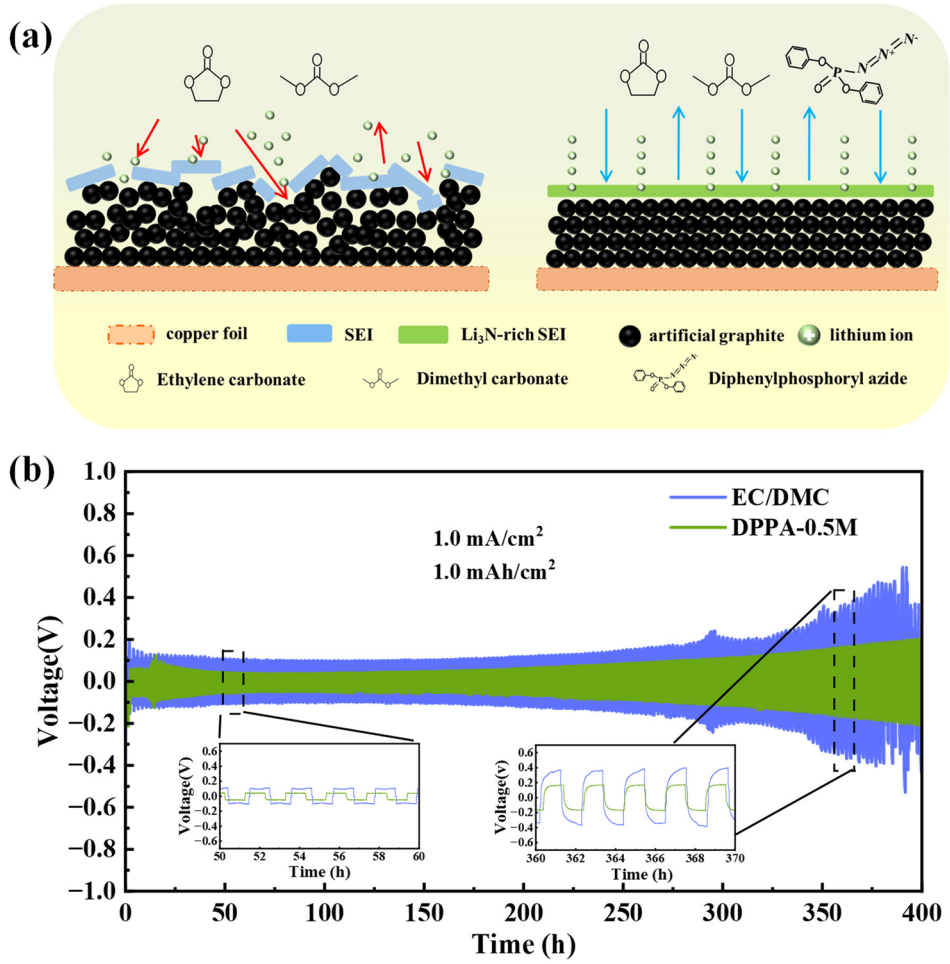

Figure 4. (**a**) Schematic diagram of graphite electrodes in different electrolytes. (**b**) The time–voltage curves of Li//Li battery cycle test.

At last, we used an electric heating plate, cone calorimetry, thermocouples, infrared thermal imaging and digital camera to test the fire risk of AG//LFP pouch cells with and without DPPA (the detailed process was recorded in Videos S4 and S5, Supplementary Materials). As shown in Figure 6a, with continuous external heating, the pouch cell using EC/DMC broke at 200 s and released a large amount of white smoke, which was mainly from the thermal decomposition of lithium salts and carbonate electrolytes. After the white smoke release phase, the pouch cell shell began to carbonize and continued to heat up. At 267 s, the pouch cell caught fire and sent out a huge flame instantly. The temperature variation trend of the pouch cell surface can be observed in real time through the thermocouple curves (Figure 6c), and the temperature of the pouch cell shell soared from 230 °C to 630 °C. After the electrolyte and other combustible substances burned out, the flame went out and the pouch cell cooled down. As shown in Figure 6b, the pouch cell using DPPA-0.5M was observed under the same external conditions, and the pouch cell released white smoke at 210 s. At 320 s, the pouch cell caught fire, but the fire was small. The maximum temperature of the shell surface was 500 °C. There was no significant spike in temperature, and then it entered the cooling process. The results of digital video, thermal imaging and thermocouple curves of the whole combustion process are consistent. The heat release rate (HRR) is a key index to evaluate the fire risk. As shown in Figure 6d, the peak HRR of the pouch cell using EC/DMC reached 716 KW/m^2. In contrast, the peak

HRR of the pouch cell using DPPA-0.5M was low. Similarly, the peak CO_2 release rate reached 66 mg/s when the pouch cell using EC/DMC caught fire, but the peak CO_2 release rate of the pouch cell using DPPA-0.5M was 26 mg/s (Figure 6e). Overall, after DPPA was added to the electrolyte, the peak HRR of the pouch cell reduced by 46.1%, the maximum combustion temperature reduced by 22.5% and the peak CO_2 release rate reduced by 61.2%. This work compared the total heat release (THR) and total smoke release (TSR) of the fire, as shown in Figure S6. Compared with EC/DMC, the THR of the pouch cell with DPPA-0.5M reduced by 48.4% and the TSR reduced by 83.7%. The burnt cell residue was tested by XRD, as shown in Figure S7. The residue mainly contains lithium carbonate, lithium oxide, aluminum, LFP, etc. The above results indicate that DPPA as an electrolyte additive plays a very good flame-retardant role and inhibits the high HRR of cell combustion to reduce the risk of fire.

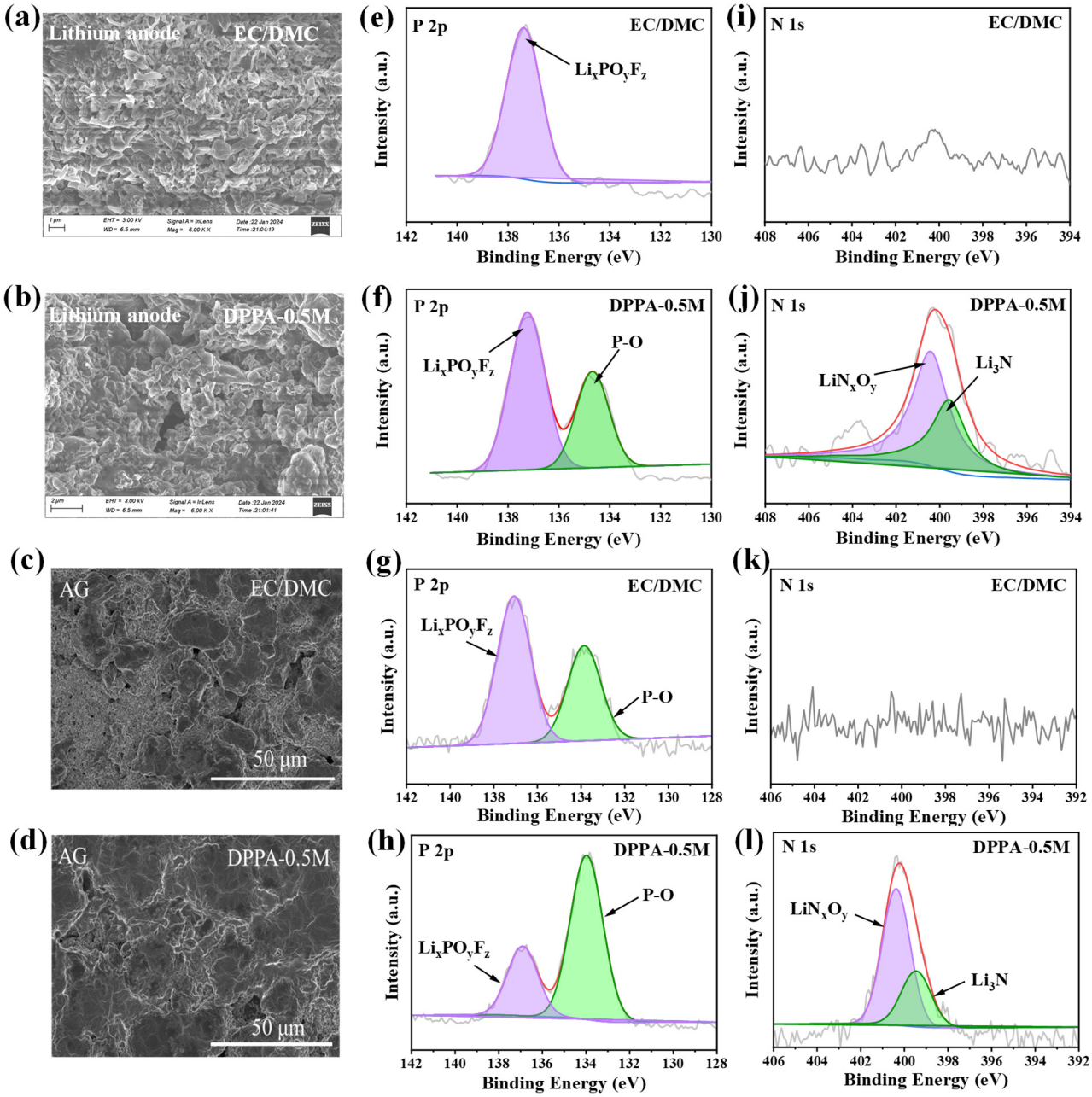

Figure 5. SEM image of lithium anode of Li//Li batteries after cycle: (**a**) EC/DMC (**b**) DPPA-0.5M. SEM image of AG electrode of AG//Li half cells after cycle (**c**) EC/DMC (**d**) DPPA-0.5M. The XPS analysis results of the above electrode surface are (**e**–**h**) P 2p (**i**–**l**) N 1s.

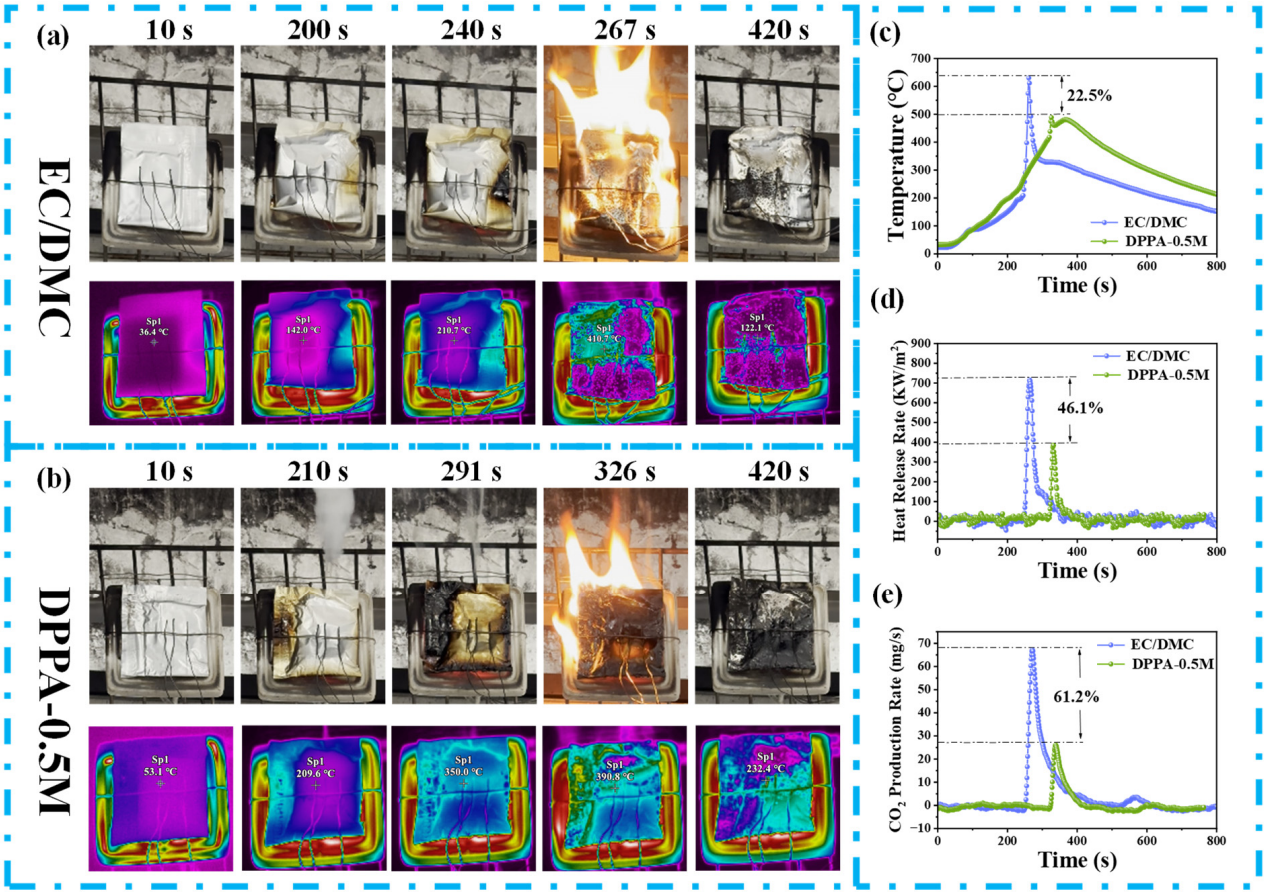

Figure 6. Fire risk test for pouch cells of AG//LFP using commercial EC/DMC or DPPA-0.5M electrolytes. Digital photos of the test process and corresponding infrared thermal imaging image screenshots (**a**) EC/DMC and (**b**) DPPA-0.5M. (**c**) Time–temperature curves. (**d**) Heat release rate results. (**e**) CO_2 release rate curves of the pouch cells during heating.

4. Conclusions

We developed DPPA as a flame-retardant multifunctional electrolyte additive for lithium-ion batteries. In terms of safety, the SET value of the electrolyte was 20 s/g when the DPPA concentration was 0.5M, providing satisfactory flame retardancy. DPPA also contributed to the construction of a Li_3N-rich SEI, which facilitated the transfer and uniform deposition of Li^+. This ensured the protection of the graphite structure and inhibition of lithium dendrites, leading to better electrochemical performance. The AG//Li half cells with DPPA-0.5M maintained a specific capacity of 350 mAh/g after 200 cycles at a current density of 0.2 C, and the surface microstructure of the AG electrode was regular. With loose lithium dendrites and regular blocky morphology, the surface of the lithium metal electrode was also relatively flat. The cycle performance and rate performance of LFP//Li half cells with DPPA-0.5M were tested, and their performance was comparable to the cells with commercial EC/DMC. The safety of the pouch cells using DPPA was further demonstrated by the fire risk test. The pouch cell had low peak HRR because of the excellent flame retardancy performance of DPPA. In summary, the DPPA can improve the safety and electrochemical performance of lithium-ion batteries and protect the graphite anode. Our research provides a simple and feasible direction for the development of safe and efficient lithium-ion batteries.

Supplementary Materials: The following supporting information can be downloaded at: https://www.mdpi.com/article/10.3390/batteries10040117/s1, Figure S1: The complete contact angle test results of separator and electrolytes; Figure S2: Digital photos of separator and electrolytes; Figure S3: LSV curve of the EC/DMC and electrolyte with DPPA at a scan rate of 1.0 mV s^{-1} between 2.5 V and 6.0 V; Figure S4: CV curves of AG//Li cells using electrolytes with and without DPPA in the voltage range of 0–2.0 V (a) EC/DMC (b) DPPA-0.1M (c) DPPA-0.2M (d) DPPA-0.5M (e) DPPA-1.0M (f) DPPA-1.5M, the scanning rate is 0.2 mV s^{-1}; Figure S5: The content comparison of various elements in SEI; Figure S6: (a) THR (b) TSR; Figure S7: XRD patterns of the post-combustion residue; Video S1: The combustion behavior of EC/DMC; Video S2: The combustion behavior of DPPA-0.5M; Video S3: The combustion behavior of DPPA-1.0M; Video S4: Fire risk test for pouch cells with EC/DMC; Video S5: Fire risk test for pouch cells with DPPA-0.5M.

Author Contributions: Z.L. completed experimental design, data processing and draft writing. C.L. and L.H. were involved in methodology, reviewing and editing. Y.K. and Y.H. performed conceptualization, formal analysis, supervision and acquired funding. All authors have read and agreed to the published version of the manuscript.

Funding: This work was supported by Key Research & Development (R&D) Plan of Anhui Province under Grant (No. 2022a05020019, No. 2023z04020017) and the Fundamental Research Funds for the Central Universities (WK2320000057).

Data Availability Statement: The original contributions presented in the study are included in the article/Supplementary Material, further inquiries can be directed to the corresponding authors.

Conflicts of Interest: The authors declare no conflict of interest.

References

1. Li, N.; Xie, K.; Huang, H. Ferroelectric Materials for High Energy Density Batteries: Progress and Outlook. *ACS Energy Lett.* **2023**, *8*, 4357–4370. [CrossRef]
2. Armand, M.; Tarascon, J.M. Building better batteries. *Nature* **2008**, *451*, 652–657. [CrossRef] [PubMed]
3. Choi, J.W.; Aurbach, D. Promise and reality of post-lithium-ion batteries with high energy densities. *Nat. Rev. Mater.* **2016**, *16*, 16013. [CrossRef]
4. Choi, N.S.; Chen, Z.; Freunberger, S.A.; Ji, X.; Sun, Y.K.; Amine, K.; Yushin, G.; Nazar, L.F.; Cho, J.; Bruce, P.G. Challenges Facing Lithium Batteries and Electrical Double-Layer Capacitors. *Angew. Chem. Int. Ed.* **2012**, *51*, 9994–10024. [CrossRef] [PubMed]
5. Ning, J.; Duan, K.; Wang, K.; Liu, J.; Wang, S.; Zhang, J. Boosting practical high voltage lithium metal batteries by butyronitrile in ether electrolytes via coordination, hydrolysis of C N and relatively mild concentration strategy. *J. Energy Chem.* **2022**, *67*, 290–299. [CrossRef]
6. Chen, K.; Yang, H.; Liang, F.; Xue, D. Microwave-Irradiation-Assisted Combustion toward Modified Graphite as Lithium Ion Battery Anode. *ACS Appl. Mater. Interfaces* **2018**, *10*, 909–914. [CrossRef] [PubMed]
7. Heng, S.; Shan, X.; Wang, W.; Wang, Y.; Zhu, G.; Qu, Q.; Zheng, H. Controllable solid electrolyte interphase precursor for stabilizing natural graphite anode in lithium ion batteries. *Carbon* **2020**, *159*, 390–400. [CrossRef]
8. Gogoi, N.; Bowall, E.; Lundström, R.; Mozhzhukhina, N.; Hernández, G.; Broqvist, P.; Berg, E.J. Silyl-Functionalized Electrolyte Additives and Their Reactivity toward Lewis Bases in Li-Ion Cells. *Chem. Mater.* **2022**, *34*, 3831–3838. [CrossRef]
9. Han, X.; Chen, J.; Chen, M.; Zhou, W.; Zhou, X.; Wang, G.; Wong, C.-P.; Liu, B.; Luo, L.; Chen, S.; et al. Induction of planar Li growth with designed interphases for dendrite-free Li metal anodes. *Energy Storage Mater.* **2021**, *39*, 250–258. [CrossRef]
10. Lee, T.; Kim, N.; Lee, J.; Lee, Y.; Sung, J.; Kim, H.; Chae, S.; Cha, H.; Son, Y.; Kwak, S.K.; et al. Suppressing Deformation of Silicon Anodes via Interfacial Synthesis for Fast-Charging Lithium-Ion Batteries. *Adv. Energy Mater.* **2023**, *13*, 2301139. [CrossRef]
11. Wang, H.; Zhu, Y.; Kim, S.C.; Pei, A.; Li, Y.; Boyle, D.T.; Wang, H.; Zhang, Z.; Ye, Y.; Huang, W.; et al. Underpotential lithium plating on graphite anodes caused by temperature heterogeneity. *Proc. Natl. Acad. Sci. USA* **2020**, *117*, 29453–29461. [CrossRef] [PubMed]
12. Zhang, L.; Tsolakidou, C.; Mariyappan, S.; Tarascon, J.-M.; Trabesinger, S. Unraveling gas evolution in sodium batteries by online electrochemical mass spectrometry. *Energy Storage Mater.* **2021**, *42*, 12–21. [CrossRef]
13. Zheng, H.; Xiang, H.; Jiang, F.; Liu, Y.; Sun, Y.; Liang, X.; Feng, Y.; Yu, Y. Lithium Difluorophosphate-Based Dual-Salt Low Concentration Electrolytes for Lithium Metal Batteries. *Adv. Energy Mater.* **2020**, *10*, 2001440. [CrossRef]
14. Dong, J.; Dai, H.; Fan, Q.; Lai, C.; Zhang, S. Grain refining mechanisms: Initial levelling stage during nucleation for high-stability lithium anodes. *Nano Energy* **2019**, *66*, 104128. [CrossRef]
15. Fang, C.; Ye, Z.; Wang, Y.; Zhao, X.; Huang, Y.; Zhao, R.; Liu, J.; Han, J.; Huang, Y. Immobilizing an organic electrode material through π–π interaction for high-performance Li-organic batteries. *J. Mater. Chem. A* **2019**, *7*, 22398–22404. [CrossRef]
16. Gao, X.; Zhou, Y.-N.; Han, D.; Zhou, J.; Zhou, D.; Tang, W.; Goodenough, J.B. Thermodynamic Understanding of Li-Dendrite Formation. *Joule* **2020**, *4*, 1864–1879. [CrossRef]

17. Liu, Y.; Zhu, Y.; Cui, Y. Challenges and opportunities towards fast-charging battery materials. *Nat. Energy* **2019**, *4*, 540–550. [CrossRef]
18. Liu, J.; He, S.; Liu, S.; Wang, S.; Zhang, J. Advanced electrolyte systems with additives for high-cell-voltage and high-energy-density lithium batteries. *J. Mater. Chem. A* **2022**, *10*, 22929–22954. [CrossRef]
19. Giffin, G.A. The role of concentration in electrolyte solutions for non-aqueous lithium-based batteries. *Nat. Commun.* **2022**, *13*, 5250. [CrossRef]
20. Liao, C.; Han, L.; Wang, W.; Li, W.; Mu, X.; Kan, Y.; Zhu, J.; Gui, Z.; He, X.; Song, L.; et al. Non-Flammable Electrolyte with Lithium Nitrate as the Only Lithium Salt for Boosting Ultra-Stable Cycling and Fire-Safety Lithium Metal Batteries. *Adv. Funct. Mater.* **2023**, *33*, 2212605. [CrossRef]
21. Han, L.; Liao, C.; Mu, X.; Wu, N.; Xu, Z.; Wang, J.; Song, L.; Kan, Y.; Hu, Y. Flame-Retardant ADP/PEO Solid Polymer Electrolyte for Dendrite-Free and Long-Life Lithium Battery by Generating Al, P-rich SEI Layer. *Nano Lett.* **2021**, *21*, 4447–4453. [CrossRef]
22. Han, L.; Liu, Y.; Liao, C.; Zhao, Y.; Cao, Y.; Kan, Y.; Zhu, J.; Hu, Y. Noncombustible 7 μm-thick solid polymer electrolyte for highly energy density solid state lithium batteries. *Nano Energy* **2023**, *12*, 108448. [CrossRef]
23. Han, B.; Zhang, Z.; Zou, Y.; Xu, K.; Xu, G.; Wang, H.; Meng, H.; Deng, Y.; Li, J.; Gu, M. Poor Stability of Li2CO3 in the Solid Electrolyte Interphase of a Lithium-Metal Anode Revealed by Cryo-Electron Microscopy. *Adv. Mater.* **2021**, *33*, 2100404. [CrossRef]
24. Peled, E.; Menkin, S. Review—SEI: Past, Present and Future. *J. Electrochem. Soc.* **2017**, *164*, A1703–A1719. [CrossRef]
25. Tan, J.; Matz, J.; Dong, P.; Shen, J.; Ye, M. A Growing Appreciation for the Role of LiF in the Solid Electrolyte Interphase. *Adv. Energy Mater.* **2021**, *11*, 2100046. [CrossRef]
26. Sun, Y.; Li, Y.; Sun, J.; Li, Y.; Pei, A.; Cui, Y. Stabilized Li_3N for efficient battery cathode prelithiation. *Energy Storage Mater.* **2017**, *6*, 119–124. [CrossRef]
27. Ye, L.; Liao, M.; Wang, B.; Peng, H. Regulating Interfacial Lithium Ion by Artificial Protective Overlayers for High-Performance Lithium Metal Anodes. *Chem. A Eur. J.* **2022**, *28*, 202103300. [CrossRef] [PubMed]
28. Li, Y.; Sun, Y.; Pei, A.; Chen, K.; Vailionis, A.; Li, Y.; Zheng, G.; Sun, J.; Cui, Y. Robust Pinhole-free Li_3N Solid Electrolyte Grown from Molten Lithium. *ACS Cent. Sci.* **2017**, *4*, 97–104. [CrossRef]
29. Chen, K.; Pathak, R.; Gurung, A.; Adhamash, E.A.; Bahrami, B.; He, Q.; Qiao, H.; Smirnova, A.L.; Wu, J.J.; Qiao, Q.; et al. Flower-shaped lithium nitride as a protective layer via facile plasma activation for stable lithium metal anodes. *Energy Storage Mater.* **2019**, *18*, 389–396. [CrossRef]
30. Park, K.; Goodenough, J.B. Dendrite-Suppressed Lithium Plating from a Liquid Electrolyte via Wetting of Li_3N. *Adv. Energy Mater.* **2017**, *7*, 1700732. [CrossRef]
31. Hwang, J.-Y.; Park, S.-J.; Yoon, C.S.; Sun, Y.-K. Customizing a Li–metal battery that survives practical operating conditions for electric vehicle applications. *Energy Environ. Sci.* **2019**, *12*, 2174–2184. [CrossRef]
32. Kang, D.; Xiao, M.; Lemmon, J.P. Artificial Solid-Electrolyte Interphase for Lithium Metal Batteries. *Batter. Supercaps* **2020**, *4*, 445–455. [CrossRef]
33. Kim, M.S.; Ryu, J.-H.; Deepika; Lim, Y.R.; Nah, I.W.; Lee, K.-R.; Archer, L.A.; Il Cho, W. Langmuir–Blodgett artificial solid-electrolyte interphases for practical lithium metal batteries. *Nat. Energy* **2018**, *3*, 889–898. [CrossRef]
34. Wang, T.H.; Chen, C.; Li, N.W.; Su, K.; Wu, X.; Yu, L.; Chen, X.C. Cations and anions regulation through hybrid ionic liquid electrolytes towards stable lithium metal anode. *Chem. Eng. J.* **2022**, *439*, 135780. [CrossRef]
35. Weng, S.; Yang, G.; Zhang, S.; Liu, X.; Zhang, X.; Liu, Z.; Cao, M.; Ateş, M.N.; Li, Y.; Chen, L.; et al. Kinetic Limits of Graphite Anode for Fast-Charging Lithium-Ion Batteries. *Nano-Micro Lett.* **2023**, *15*, 215. [CrossRef] [PubMed]
36. Ye, S.; Wang, L.; Liu, F.; Shi, P.; Wang, H.; Wu, X.; Yu, Y. g-C3N4Derivative Artificial Organic/Inorganic Composite Solid Electrolyte Interphase Layer for Stable Lithium Metal Anode. *Adv. Energy Mater.* **2020**, *10*, 202002647. [CrossRef]
37. Zhu, J.; Chen, J.; Luo, Y.; Sun, S.; Qin, L.; Xu, H.; Zhang, P.; Zhang, W.; Tian, W.; Sun, Z. Lithiophilic metallic nitrides modified nickel foam by plasma for stable lithium metal anode. *Energy Storage Mater.* **2019**, *23*, 539–546. [CrossRef]
38. Li, S.; Li, J.; Wang, P.; Ding, H.; Zhou, J.; Li, C.; Cui, X. Interface Engineering Regulation by Improving Self-Decomposition of Lithium Salt-Type Additive using Ultrasound. *Adv. Funct. Mater.* **2023**, *34*, 2307180. [CrossRef]
39. Liao, C.; Han, L.; Mu, X.; Zhu, Y.; Wu, N.; Lu, J.; Zhao, Y.; Li, X.; Hu, Y.; Kan, Y.; et al. Multifunctional High-Efficiency Additive with Synergistic Anion and Cation Coordination for High-Performance $LiNi_{0.8}Co_{0.1}Mn_{0.1}O_2$ Lithium Metal Batteries. *ACS Appl. Mater. Interfaces* **2021**, *13*, 46783–46793. [CrossRef]
40. Zhao, W.; Zheng, G.; Ji, Y.; Peng, C.; Ren, F.; Liu, M.; Pan, F.; Yang, Y. Modulation and quantitative study of conformal electrode-electrolyte interfacial chemistry toward high-energy-density $LiNi_{0.6}Co_{0.2}Mn_{0.2}O_2$||SiO-C pouch cells. *Energy Storage Mater.* **2022**, *53*, 424–434. [CrossRef]
41. Mu, X.; Li, X.; Liao, C.; Yu, H.; Jin, Y.; Yu, B.; Han, L.; Chen, L.; Kan, Y.; Song, L.; et al. Phosphorus-Fixed Stable Interfacial Nonflammable Gel Polymer Electrolyte for Safe Flexible Lithium-Ion Batteries. *Adv. Funct. Mater.* **2022**, *32*, 2203006. [CrossRef]
42. Gachot, G.; Ribière, P.; Mathiron, D.; Grugeon, S.; Armand, M.; Leriche, J.B.; Pilard, S.; Laruelle, S. Gas Chromatography/Mass Spectrometry As a Suitable Tool for the Li-Ion Battery Electrolyte Degradation Mechanisms Study. *Anal. Chem.* **2011**, *83*, 478–485. [CrossRef] [PubMed]
43. Shi, P.; Zhang, L.; Xiang, H.; Liang, X.; Sun, Y.; Xu, W. Lithium Difluorophosphate as a Dendrite-Suppressing Additive for Lithium Metal Batteries. *ACS Appl. Mater. Interfaces* **2018**, *10*, 22201–22209. [CrossRef] [PubMed]

44. Fu, J.; Ji, X.; Chen, J.; Chen, L.; Fan, X.; Mu, D.; Wang, C. Lithium Nitrate Regulated Sulfone Electrolytes for Lithium Metal Batteries. *Angew. Chem. Int. Ed.* **2020**, *59*, 22194–22201. [CrossRef]
45. Tan, S.J.; Yue, J.; Hu, X.C.; Shen, Z.Z.; Wang, W.P.; Li, J.Y.; Zuo, T.T.; Duan, H.; Xiao, Y.; Yin, Y.X.; et al. Nitriding-Interface-Regulated Lithium Plating Enables Flame-Retardant Electrolytes for High-Voltage Lithium Metal Batteries. *Angew. Chem. Int. Ed.* **2019**, *58*, 7802–7807. [CrossRef]